STATUS REPORT FOR NASA GRANT NAG1-1177

Steven A. Ackerman and William L. Smith

Cooperative Institute for Meteorological Satellite Studies

University of Wisconsin-Madison, Madison, WI 53706

(June 1991)

Over the past year, our FIRE related research at the CIMSS has focused primarily on three activities: a modeling effort, analysis of HIS data collected during FIRE I, and preparation for the field phase of FIRE II. These efforts are discussed separately below.

MODELING EFFORTS

A radiative transfer model has been developed which can be used to simulate measurements made from an aircraft or ground based HIS. The theoretical model will be used to simulate HIS observed radiances in which the cloud and atmospheric properties are known and is therefore essential for the development and verification of algorithms for retrieving cloud radiative properties. The model is a coupling of FASCOD2 with a multiple scattering code. FASCOD2 is used to determine the clear air radiance and transmittance above and below the cloud layer and the gaseous transmittance within the cloud. Multiple scattering by the cloud layer is handled with a doubling/adding model. The model is briefly discussed below.

Assuming a plane-parallel horizontally-homogeneous cloud, the IR radiative transfer equation is:

$$\mu \frac{\mathrm{d}I(\delta,\mu)}{\mathrm{d}\delta} = I(\delta,\mu) - (1-\omega_0)B(T) - \frac{\omega_0}{2}\int_{-1}^{1} P(\delta,\mu,\mu')I(\delta,\mu')\mathrm{d}\mu' \qquad (1)$$

where $I(\delta,\mu)$ is the azimuthally-averaged monochromatic intensity, δ is the optical thickness, ω_0 is the single scattering albedo, $P(\delta,\mu,\mu')$ is the azimuthally averaged phase function, B(T) represents

the Planck function at temperature T, and $\mu = cos(\theta)$ where θ is measured from downward normal direction. An accurate technique to solve Eq. (1) is the doubling-adding method. This type of model has been discussed in detail in previous atmospheric studies (Grant and Hunt, 1969; Wiscombe, 1976 a and b, 1977; and Stephens, 1978, 1980). We assumed that the model cloud is composed of equivalent spherical ice particles (or water drops) or ice particles of cylindrical shape.

The phase function used in Eq.(1) is Henyen-Greenstein phase function

$$P(\mu^*) = \frac{1-g^2}{(1+g-2g\mu^*)^{\frac{3}{2}}} \tag{2}$$

where μ^* is the scatter angle (defined as the angle between the incident and scattered beams). The parameter g is the asymmetry factor for this phase function. The asymmetry factor g together with the extinction coefficient σ_{ext} (used to define the optical thickness), and the single scatter albedo ω_0 are crucial to the solution of Eq.(1). Based on Mie scatter theory, these parameters are calculated over the HIS spectral region with various effective particle radii. Calculations have also been conducted for cylindrical shaped particles in order to test the sensitivity of retrieval algorithms to particle shape.

A plane-parallel model atmosphere consisting of three layers (cloud, above and below cloud) is employed to evaluate the transfer of thermal infrared radiation. The specified temperature and water vapor profiles are taken from observed temperature and moisture profiles. The calculation of the transfer of infrared radiance through cloudy atmosphere is carried out for 16 discrete emergent angles, including nadir. The radiances emitted by the surface or atmosphere below and above the cloud layer were generated from FASCOD2. In the computation of the cloud layer radiance contribution, the effect of water vapor within clouds is taken into consideration. As a result, the asymmetry parameter and the single scattering albedo of the cloud layer are expressed as

$$g' = \frac{g\delta_c + \delta_g}{\delta_c + \delta_g} \tag{3}$$

and

$$\omega_0' = \frac{\omega_0 \delta_c}{\delta_c + \delta_g} \tag{4}$$

where δ_c and δ_g represent cloud and gaseous optical thickness respectively. In addition to simulating a cloud radiance spectrum, the multiple scattering model is also used to specify the vertical beam emissivity and beam reflectivity spectra of the cloud. Calculations for clouds consisting of spheres and cylinders of various sizes have been conducted for which retrieval algorithms can be applied. The model is also used to calculate cloud effective temperatures.

Examples of theoretical calculations of cirrus clouds consisting of cylinders of two different size distributions are depicted in Figures 1 and 2 for different ice water contents (IWC) (thin- 0.001 g m^{-3}, moderate- 0.01 g m^{-3}, and thick- 0.1 g m^{-3}). These calculations are being used to verify the retrieval techniques proposed by Ackerman *et al.* (1990) and a new method developed by Smith *et al* (1991).

RETRIEVAL ALGORITHMS

The 8-12 μm spectral region is an important atmospheric window for radiometric studies of the earth's surface and clouds. Selective gaseous absorption in this window occurs in the 9.6 μm ozone band with the remaining absorption dominated by water-vapor. This spectral window is also very important for climate studies since most of the earth/atmosphere longwave radiative loss to space occurs in this spectral region. Cirrus clouds have a large impact on the attenuation of radiation in this atmospheric window region (Platt 1973; Liou 1974; Stephens 1980; Wu 1984). Understanding the interaction of cirrus clouds with the radiation field is critically important for climate studies and in interpretating satellite radiometric measurements. This understanding is hampered by the large variability of cirrus optical properties, making it difficult to determine their presence, let alone their radiative impact. A technique of determining cloud spectral emissivity and reflectivity in the 8-12 μm region based on observations from a High-resolution Michelson Interferometer was proposed and applied to FIRE data by Ackerman *et al.* (1990). We have applied this algorithm to HIS radiances simulated with the theoretical model. The retrieval of

cloud emissivity by this method makes use of lidar data, to specify cloud top and base height, and HIS to derive the spectral effective beam emissivity (Platt and Stephens, 1980) of cirrus clouds. The radiances observed by the HIS can be expressed, neglecting scattering processes, as

$$I(Z_A) = B(T_S)\tau(Z_A,0) + \int_0^{Z_A} B[T(Z)]\frac{d\tau(Z_A,Z)}{dz}dz \tag{5}$$

where $B(T_S)$ is Planck radiance of the surface, $\tau(Z_A,0)$ is the transmittance of the total atmosphere, and Z_A is the altitude of the aircraft (approximately 19.8 km). Separating (5) into above cloud (Z_A, Z_T), cloud (Z_T, Z_B) and below cloud (Z_B, Z_S) layers yields

$$I(Z_A) = B(T_S)\tau(Z_A,0)+\tau(Z_A,Z_B)\int_0^{Z_B} B[T(Z)]\frac{d\tau(Z_B,Z)}{dz}dz+\tau(Z_A,Z_T)\int_{Z_B}^{Z_T} B[T(Z)]\frac{d\tau(Z_T,Z)}{dz}dz + \int_{Z_T}^{Z_A} B[T(Z)]\frac{d\tau(Z_A,Z)}{dz}dz \tag{6}$$

where Z_B and Z_T are the height of cloud base and top respectively and are defined from the $B'(Z)$ profiles measured by the CALS (Spinhirne and Hart, 1989). The temperature at the cloud boundaries are determined from temperature profiles measured by a nearby radiosonde. Denoting the radiance at cloud base as

$$I(Z_B) = B[T_S]\tau(Z_B,0) + \int_0^{Z_B} B[T(Z)]\frac{d\tau(Z_B,Z)}{dz}dz \tag{7}$$

and using the Mean Value Theorem to represent the mean cloud radiance as

$$\overline{B_C} = [1-\tau(Z_T,Z_B)]^{-1}\int_{Z_B}^{Z_T} B[T(Z)]\frac{d\tau(Z_T,Z)}{dz}dz \tag{8}$$

the cloud layer transmittance is defined as

$$\tau(Z_T,Z_B) = \left[\frac{I(Z_A) - \int_{Z_T}^{Z_A} B[T(Z)]\frac{d\tau(Z_A,Z)}{dz}dz}{\tau(Z_A,Z_T)} - \overline{B_C}\right]\left[I(Z_B) - \overline{B_C}\right]^{-1} \tag{9}$$

An initial spectral transmittance of the cloud is derived by first assuming a value for $\overline{B_C}$, in this case the Planck radiance at the mid- cloud temperature. The atmospheric transmittance above

the cloud, $\tau(Z_A, Z_T)$, are computed based on the temperature and moisture profiles measured by a radiosonde launched at 1800 UTC at Greenbay WI). The above cloud contribution to the HIS observation, $\int_{Z_T}^{Z_A} B[T(Z)]\frac{d\tau(Z_A,Z)}{dz}dz$, is also theoretically determined. The clear sky HIS radiances are used to define the spectral radiance at the cloud base after subtracting the effects of the above cloud atmosphere. The measured HIS spectra are then used to calculate the transmittance from (9). These first guess cloud spectral transmittances, $\tau(Z_T, Z_B)$, are then used to solve the integral in (8). Assuming that the Planckian emission is linear in optical depth,

$$B[T(Z)] = B[T(Z_T)] + \frac{B[T(Z_B)] - B[T(Z_T)]}{\ln \tau(Z_T, Z_B)} \ln \tau(Z_T, Z) \tag{10}$$

and

$$\int_{Z_B}^{Z_T} B[T(Z)]\frac{d\tau(Z_T, Z)}{dz}dz = B[T(Z_T)] - B[T(Z_B)]\tau(Z_T, Z_B) + \frac{B[T(Z_B)] - B[T(Z_T)]}{\ln \tau(Z_T, Z_B)}(\tau(Z_T, Z_B) - 1) \tag{11}$$

Equation (11) and the initial estimate of $\tau(Z_T, Z_B)$ are then used to calculate a corrected value of $\overline{B_C}$ and a new cloud transmittance is determined from (9). This iterative procedure is continued until the change in $\tau(Z_T, Z_B)$ is less than 0.003.

The results of this analysis are presented in terms of the spectral effective beam emissivity,

$$\varepsilon(Z_T, Z_B) = 1 - \tau(Z_T, Z_B) \tag{12}$$

This effective emittance is larger than the true "absorption" emittance as it includes the effects of multiple scattering within the cloud and reflection at the cloud base (Platt and Stephens, 1980). The difference between the effective emittance and the absorptance emittance is a function of the viewing angle (nadir for the HIS), the particle size and shape, and the absorption component of the optical depth (δ_a) and the temperature difference between the surface and cloud. For nadir measurements at 11.5 μm (Platt and Stephens, 1980) the difference is negligible for thin cloud, $\delta_a < 0.1$, and increases to a maximum of approximately 0.1 (15% error) at $\delta_a = 1$. The effective emissivity is used in this study to demonstrate the variability of cirrus clouds in the window region.

Examples of the effective beam emissivity derived from theoretical simulations of cirrus clouds consisting of cylindrical ice crystals are depicted in Figures 3 and 4 as a function of wavelength. The black line is the true emissivity calculated by the model, the blue line is the derived effective spectral emissivity of the cloud given the temperature and moisture profile used in the calculation, while the red and purple lines depict the retrieved effective spectral emissivity assuming an observed clear sky HIS spectra. Comparison of the black and blue lines is an indication of the "best" retrieval that can be attained using this method. Comparison of the blue with the red and purple lines indicate the errors associated with errors in the assumed clear sky values.

As expected, the retrieved emissivity overestimates the true emissivity due to the neglection of reflection and multiple scattering. The over estimation is spectrally dependent. Agreement is best between approximately 920 and 960 cm^{-1} (10.4-10.6 μm), where the effects of multiple scattering are a minimum. This is the optimum spectral region for initial estimates of the emissivity, in which scattering effects are a minimum. The slope of the spectral emissivity in this region, which is related to the particle size, is similar for the retrieved and actual emittance. Thus this is also a good spectral region for estimates of cloud particle size. Maximum errors occur in the 1100-1200 cm^{-1} band, where multiple scattering effects are a maximum. Large errors on water vapor lines in the 1100-1200 cm^{-1} (8.3-9.3 μm band) result from an incorrect water vapor/temperature profile. The high spectral resolution of the HIS allows for the retrieval between these absorption lines. Because the single scattering properties of cloud vary slowly compared to gaseous absorption, the emittance on an absorption line can be interpreted from results of adjacent wavenumbers on either side of the line. For the large particle size, there is little spectral structure to the cloud emittance, since the single scattering properties approach a limiting value. The retrieved values, however, still depict spectral structure (except for thin clouds) due to the neglection of reflection.

In addition to retrieving the cloud beam effective emissivity, the retrieval algorithm determines the cloud effective temperature. Comparisons between cloud retrieved effective temperature and model derived effective temperature are depicted in Figure 5 for two clouds, one consisting of small particles and one for large particles. The over estimation of the emissivities is compensated for by

an under estimate of the cloud effective temperature. Differences in the spectral structure of the effective temperatures are correlated with the differences in the emittance.

We have applied the retrieval method to observations collected on November 2, 1986 as a means of inferring the variability of cirrus cloud properties. We have limited the analysis of HIS observations to time periods which are coincident with the CALS lidar (provided by J. Spinherne) as well as observations from the MAMS, also known as the DR observations. This resulted in a total of 154 collocated observations. Figure 6 depicts the emittance in the 935-945 cm^{-1} band ϵ_{935} versus the difference in the emittance between the 900-907 cm^{-1} and 957-967 cm^{-1} ($\Delta\epsilon$) bands. We choose these wavelengths as they are window regions in the spectral regime where multiple scattering is a minimum, and there is a strong sensitivity to particle size. Most of the observations are for ϵ_{935} greater than 0.5. While there is large variability in $\Delta\epsilon$, we shall consider two categories divided by $\Delta\epsilon = 0.02$. Based on our theoretical calculation, $\Delta\epsilon > 0.02$ are suggestive of a cloud consisting of smaller particles. We will check the consistency of the infrared observations with visible wavelengths by comparing the HIS retrievals with observations from the MAMS.

Figure 7 depicts an image of the MAMS observations made on Nov 2, 1986 between approximately 1857 and 1906 UT. We are in the process of collocating the HIS observations with the MAMS imagery. The collocation will be checked though statistical analysis of the MAMS infrared observations with MAMS simulations using the HIS. Once the collocation has been verified we will investigate the relationship and consistency between the visible and infrared optical properties together as well as address the effects of scene variability on the HIS retrieval.

FIELD PROGRAM PREPARATION

Since the HIS last flew on the ER-2 in 1986, it has been used almost exclusively in a ground based uplooking configuration. During the period of this report the HIS has been under going reconditioning to make it flight ready on the ER-2 in preparation for FIRE II. These preparations have included calibration and alignment checks of the HIS, as well as performance evaluations.

FIGURE CAPTIONS

Figure 1. Examples of theoretical simulations of HIS observations for three cloud ice water contents for a cirrus cloud consisting of small cylinders. Thin- 0.001 g m^{-3}, moderate- 0.01 g m^{-3}, and thick- 0.1 g m^{-3}.

Figure 2. Examples of theoretical simulations of HIS observations for three cloud ice water contents for a cirrus cloud consisting of large cylinders. Thin- 0.001 g m^{-3}, moderate- 0.01 g m^{-3}, and thick- 0.1 g m^{-3}.

Figure 3. Comparison of model derived cloud emissivity and HIS spectra with retrieved emissivities for three ice water contents.

Figure 4. Same as figure 3 except for a cirrus cloud consisting of large cylindrical particles.

Figure 5. Comparison of theoretically derived effective cloud temperature with retrieved cloud effective temperature, for two cirrus clouds

Figure 6. Emittance in the 935-945 cm^{-1} band ϵ versus the difference in the emittance between the 900-907 cm^{-1} and 957-967 cm^{-1} ($\Delta\epsilon$) bands determined from HIS observations made on November 2, 1986.

Figure 7. Image of MAMS observations made on Nov 2, 1986 between approximately 1857 and 1906 UT.

REFERENCES

Ackerman, S. A., W. L. Smith, J. D. Spinhirne, and H. E. Revercomb, 1990: The 27-28 October 1986 FIRE IFO Cirrus Case Study: Spectral Properties of Cirrus Clouds in the 8-12 μm window. *Mon. Wea. Rev.*, **118, No. 11**, 2377-2388.

Grant, I. P., and G. Hunt, 1969: Discrete Space Theory of Radiative Transfer I Fundamentals, *Proc. Roy. Soc. Lond.*, **A., 313**, 183-197.

Liou, K. N., 1974: On the Radiative Properties of Cirrus in the Window Region and Their Influence on Remote Sensing of the Atmosphere, *J. Atmos. Sci.*, **31**, 522-532.

Platt, C. M. R., 1973: Lidar and Radiometric Observations of Cirrus Clouds, *J. Atmos. Sci.*, **30**, 1191-1204.

Platt, C. M. R. and G. L. Stephens, 1980: The Interpretation of Remotely Sensed High Cloud Emittances, *J. Atmos. Sci.* **37**, 2314-2322.

Revercombe, H. E., H. Buijs, H. B. Howell, D. D. Laporte, W. L. Smith and L. A. Sromovsky, 1988: Radiometric Calibration of IR Fourier Transform Spectrometers: Solution to a Problem with the High-Spectral Resolution Interferometer Sounder, *Appl. Optics*, **27**, 3210-3218.

Spinhirne, J. D. and W. D. Hart, 1990: The 27-28 October 1986 FIRE IFO cirrus case study: Cirrus Structure and Radiative Parameters from Airborne Lidar and Spectral Radiometer Observations. *J. Mon. Wea. Rev.*, **118**, 2329-2343.

Stephens, G. L., 1980: Radiative Properties of Cirrus Clouds in the Infrared Region, *J. Atmos. Sci.*, **37** ,435-445.

Wu, M. L. C., 1984: Radiative Properties and Emissivity Parameterization of High Level Thin Clouds, *J. Clim. Appl. Meteor.*, **23**, 1138-1147.

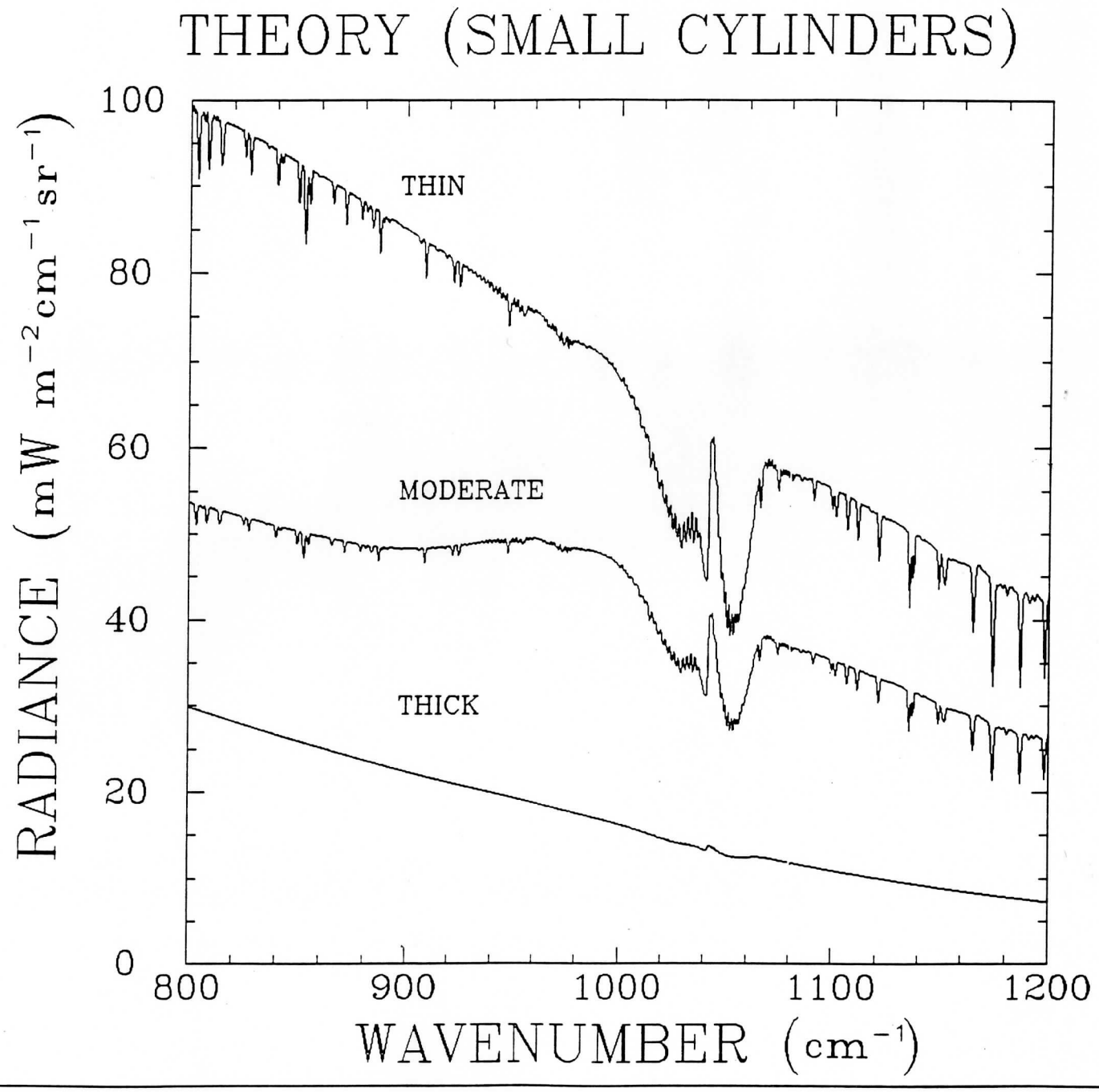

Figure 1. Examples of theoretical simulations of HIS observations for three cloud ice water contents for a cirrus cloud consisting of small cylinders. Thin- 0.001 g m^{-3}, moderate- 0.01 g m^{-3}, and thick- 0.1 g m^{-3}.

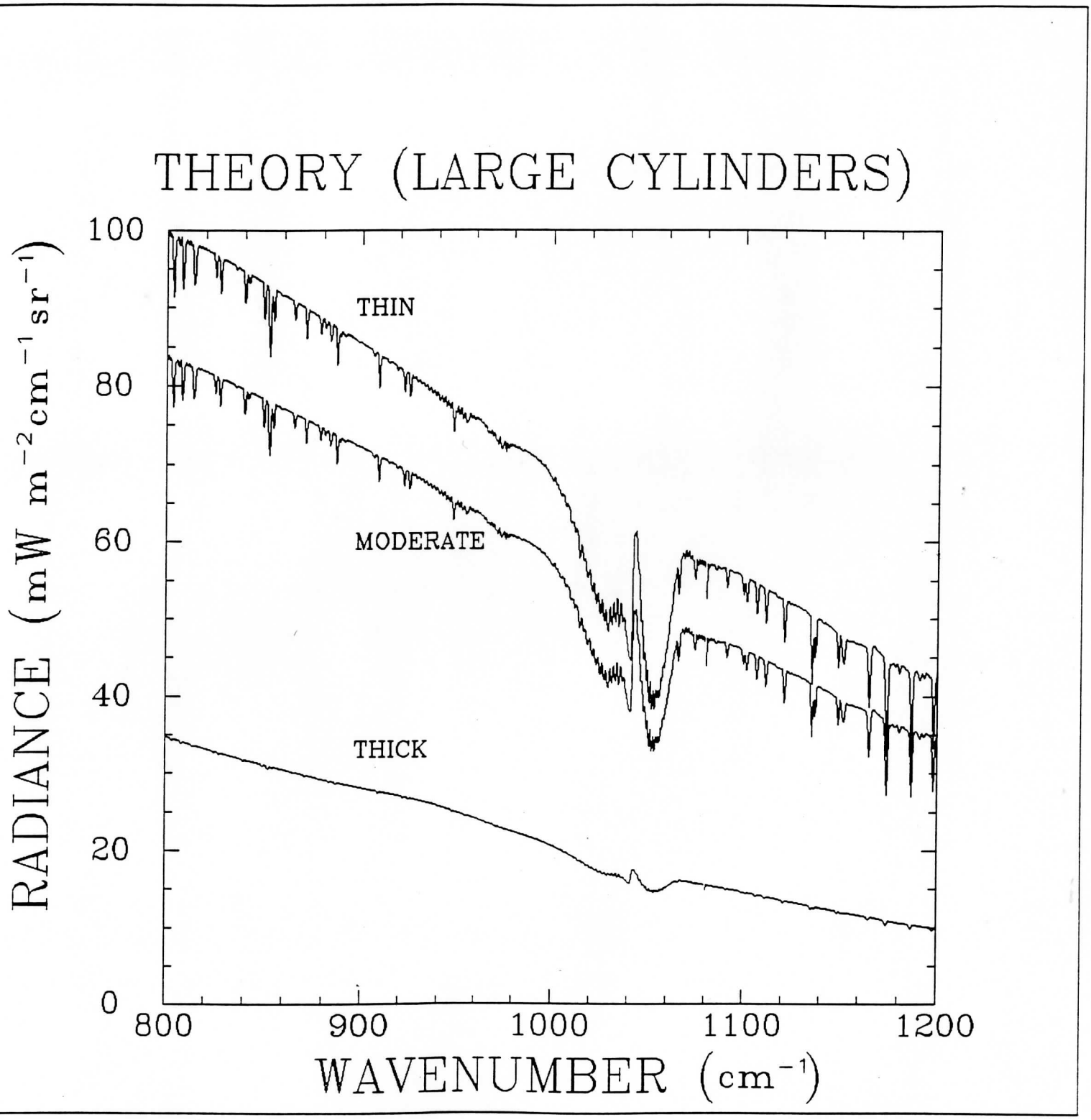

Figure 2. Examples of theoretical simulations of HIS observations for three cloud ice water contents for a cirrus cloud consisting of large cylinders. Thin- 0.001 g m^{-3}, moderate- 0.01 g m^{-3}, and thick- 0.1 g m^{-3}.

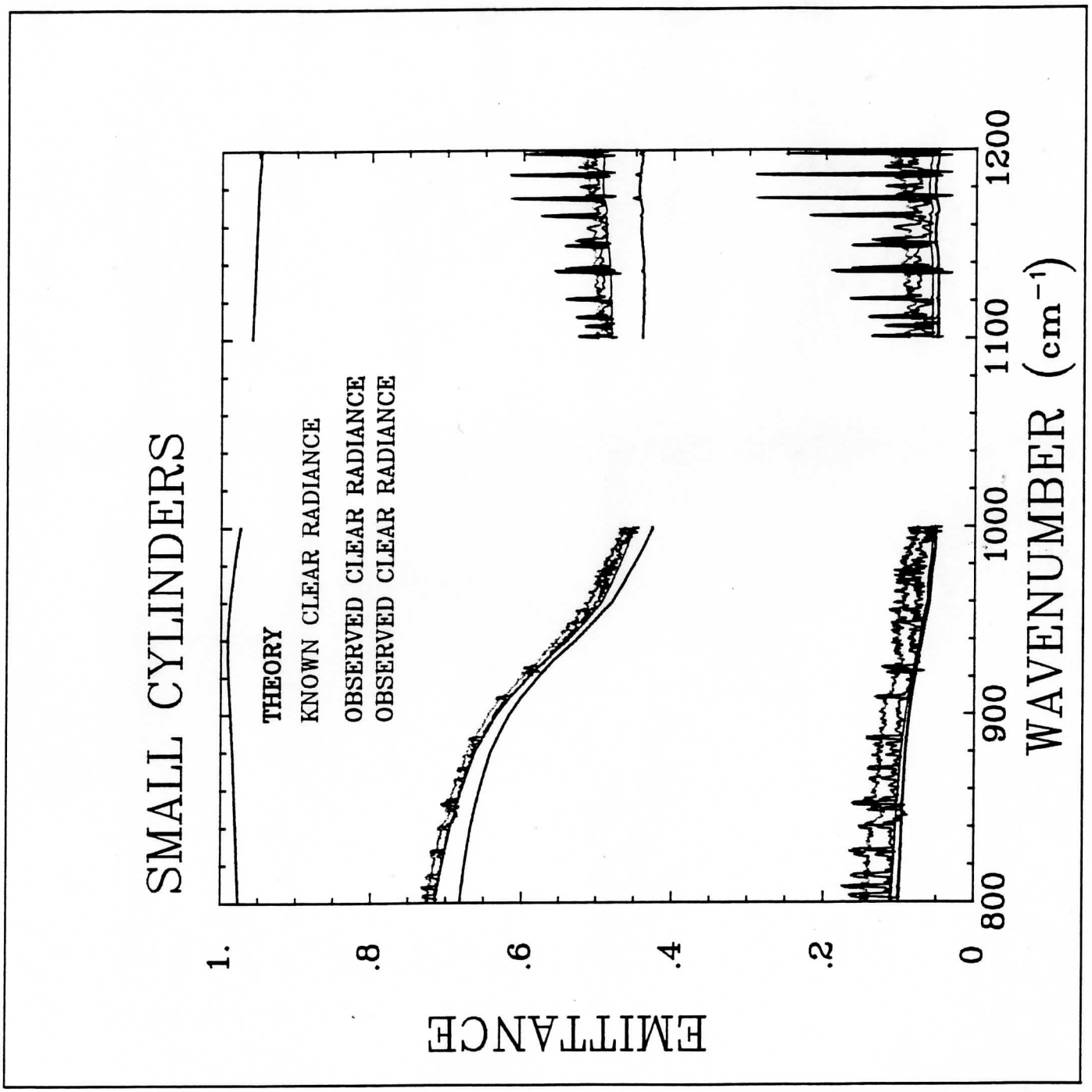

Figure 3. Comparison of model derived cloud emissivity and HIS spectra with retrieved emissivities for three ice water contents.

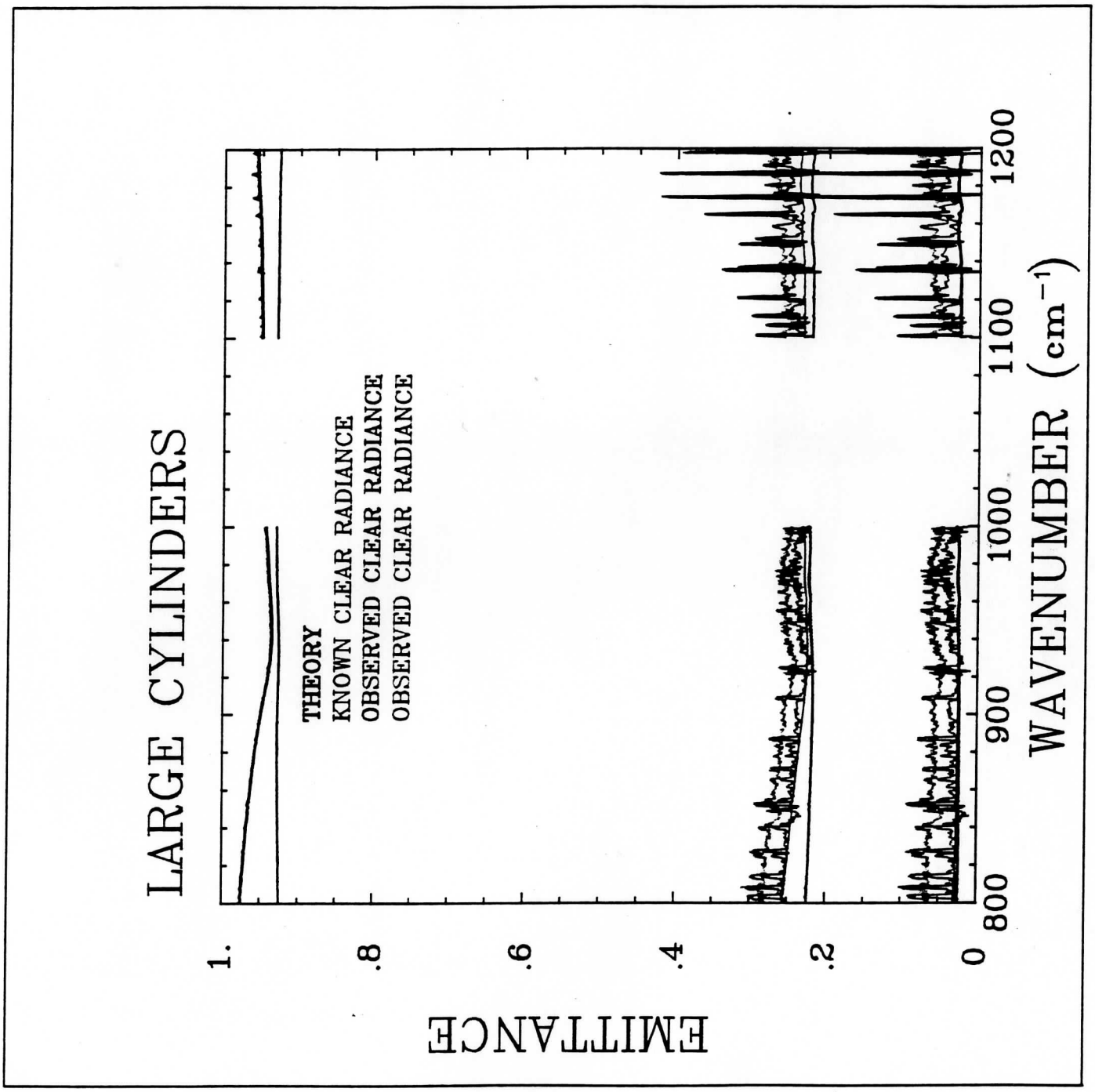

Figure 4. Same as figure 3 except for a cirrus cloud consisting of large cylindrical particles.

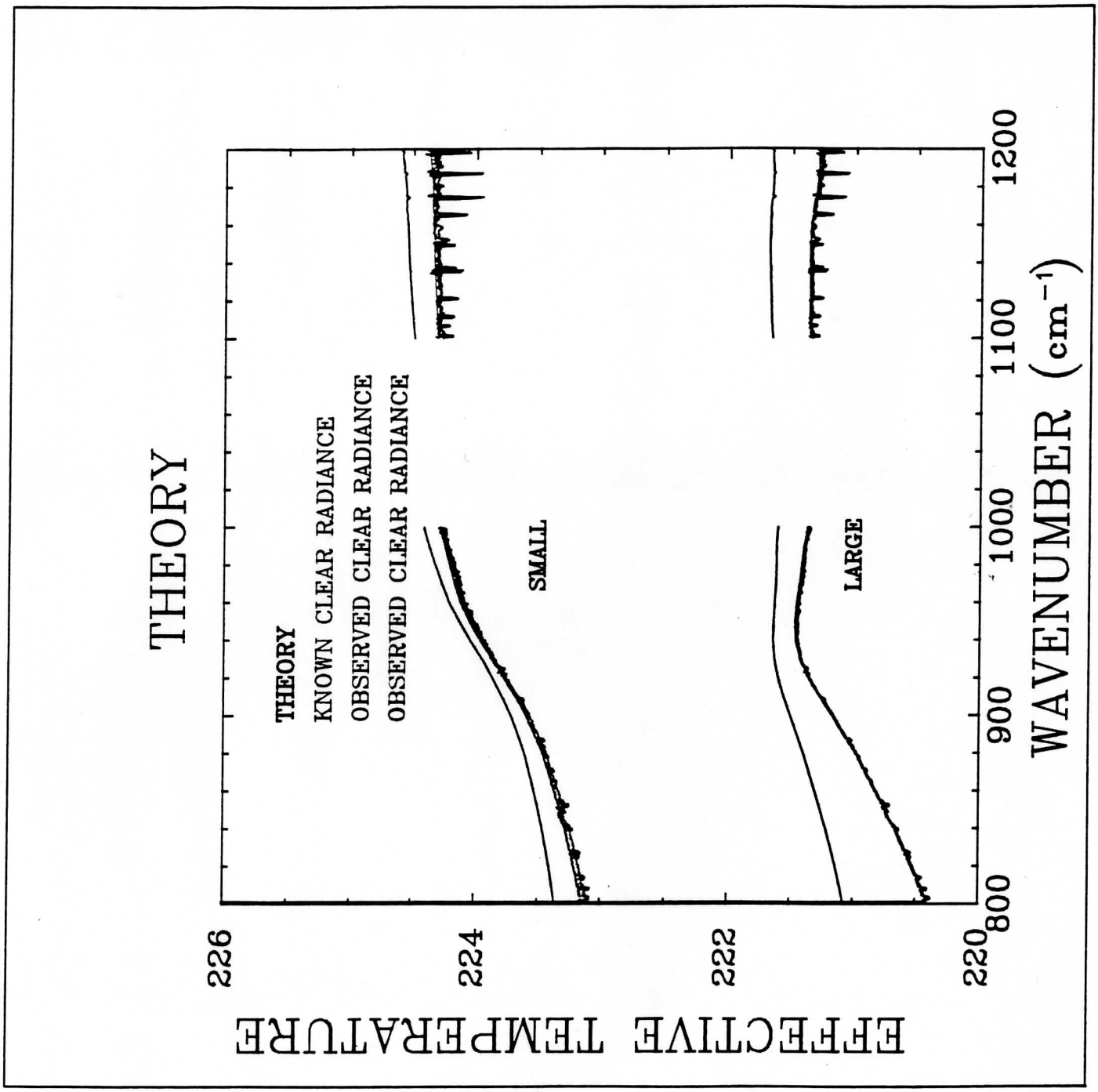

Figure 5. Comparison of theoretically derived effective cloud temperature with retrieved cloud effective temperature, for two cirrus clouds

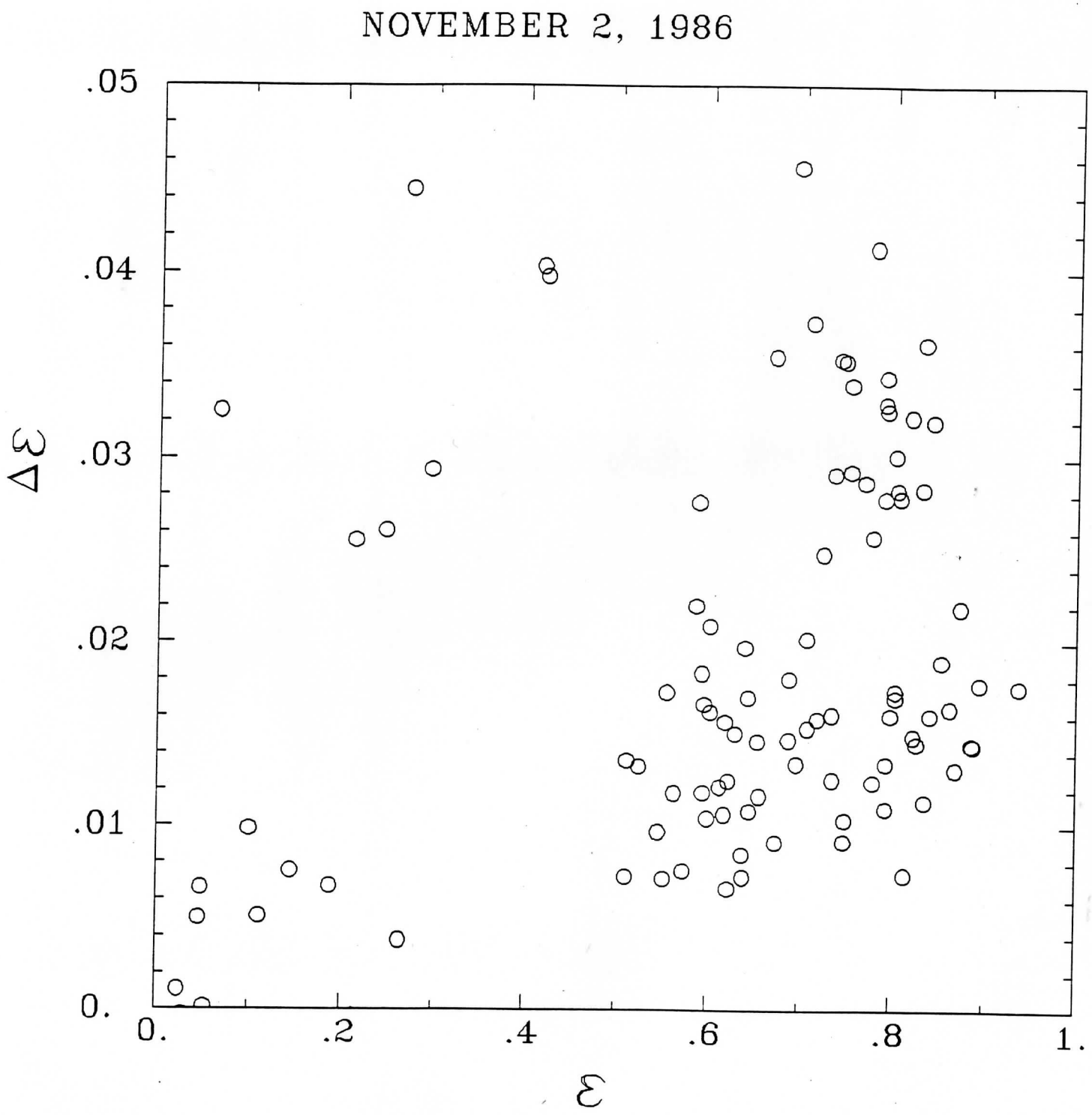

Figure 6. Emittance in the 935-945 cm^{-1} band ϵ versus the difference in the emittance between the 900-907 cm^{-1} and 957-967 cm^{-1} ($\Delta\epsilon$) bands determined from HIS observations made on November 2, 1986.

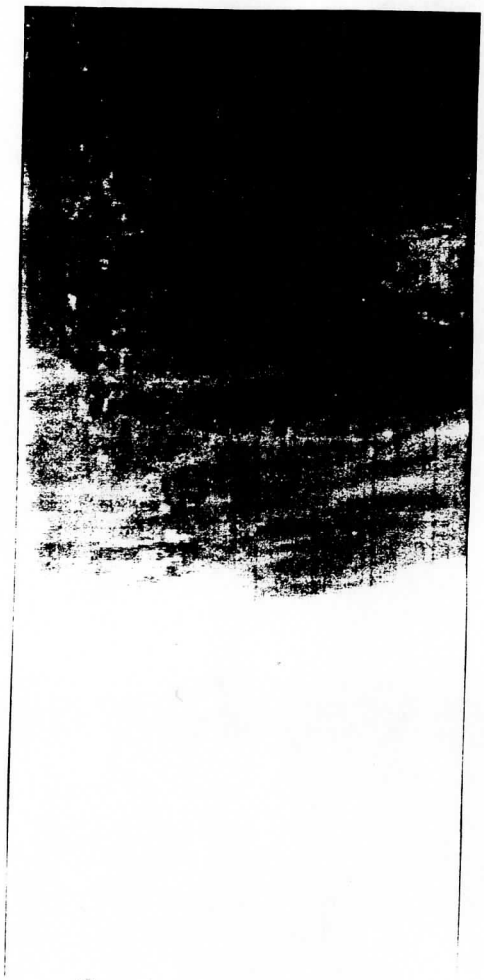

Figure 7. Image of MAMS observations made on Nov 2, 1986 between approximately 1857 and 1906 UT.